

**DESIGN, SYNTHESIS AND CHARACTERIZATION OF
THE OXYGEN REDUCTION REACTION CATALYST FOR
POLYMER ELECTROLYTE MEMBRANE FUEL CELLS**

by

Yanqi Zhang

A thesis submitted to the Faculty of the University of Delaware in partial fulfillment of the requirements for the degree of Master in Chemical Engineering

Spring 2013

© 2013 Yanqi Zhang
All Rights Reserved

**DESIGN, SYNTHESIS AND CHARACTERIZATION OF
THE OXYGEN REDUCTION REACTION CATALYST FOR
POLYMER ELECTROLYTE MEMBRANE FUEL CELLS**

by

Yanqi Zhang

Approved: _____
Yushan Yan, Ph.D.
Professor in charge of thesis on behalf of the Advisory Committee

Approved: _____
Abraham M. Lenhoff, Ph.D.
Chair of the Department of Chemical and Biomolecular Engineering

Approved: _____
Babatunde Ogunnaike, Ph.D.
Interim Dean of the College of Engineering

Approved: _____
James G. Richards, Ph.D.
Vice Provost for Graduate and Professional Education

ACKNOWLEDGMENTS

The author of the thesis appreciates her adviser Dr. Yushan Yan for all the support, knowledge and advise he has kindly offered during her master's study. The author would like to specially thank Robert Forest from Dr. Jingguang Chen's lab and Dr. David Cullen for the kind help on XPS and TEM analysis of the sample. She also thanks all her profesors, classmates and group members from graduate and undergraduate studies for the discussions, help and advise. I would like to specially thank DOE EERE for the financial support. Last but not least, to all the ones she loved and loved her, for leading her and supporting her to the day the thesis is finished.

TABLE OF CONTENTS

LIST OF FIGURES	vi
ABSTRACT	viii
Chapter	
1. INTRODUCTION	1
2. RESEARCH BACKGROUND	4
ORR Mechanism	4
ORR Activity on Pt Surface	5
Stability of Pt for ORR	7
Selective Research Activities	11
3. CATALYST OF PT SUPPORTED ON SCANDIUM OXIDE NANOSHEETS FOR PEMFC	14
Background	14
Experiment	15
Synthesis of Pt/Sc ₂ O ₃ /C Catalyst	15
Post-treatment	16
Thermal Gravimetric Analysis	16
Transmission Electron Microscopy	17
Surface Composition and Binding Strength	17
Electro-chemical Measurements	17
Results and Discussions	18
Morphology and Growth Mechanism of Pt/Sc ₂ O ₃ /C	18
ORR Activity and XPS	21
ORR Durability of Pt/Sc ₂ O ₃ /C	24
Summary	24
4. STUDY OF NANO-GOLD PARTICLES FOR ORR OF HEMFCS	26
Background	26

Experiment	27
Catalyst Preparation.....	27
Transmission Electron Microscopy	28
Electrode Preparation	28
Results and Discussions	28
Morphology	28
Cyclic Voltammetry	29
ORR Activity and Durability.....	30
Summary.....	32
5. SUMMARY AND CONCLUSION.....	33
REFERENCES	35

LIST OF FIGURES

Figure 1	Scheme of PEMFC using hydrogen as fuel and oxygen as oxidant.....	2
Figure 2	ORR mechanisms of dissociative and associative mechanism.	4
Figure 3	Free energy chart of oxygen reduction reaction on Pt surface of dissociative reaction mechanism [13].	6
Figure 4	Volcano plot of ORR activity on different metal surfaces [13].	6
Figure 5	Cell voltage (a) and Pt electrochemical surface area (b) as a function of short-stack run time. Operating condition: Hydrogen/air stoichiometric flow is 2/2, under 80 °C, 150 kPa _{abs} , 100% RH [16].	7
Figure 6	Proposed mechanisms of instability of Pt particles in low temperature fuel cells [17].	8
Figure 7	Microscopic images of PtCo/C sample with low resolution (a) before (b) after the durability test and with high resolution (c) before, (d) after and (e) overlay of the two [22].	10
Figure 8	Hundreds of elemental mapping images of the PtCo particles, (a) before and (b) after the durability test; (c) and (d) presents an example of multi-core and single-core particle respectively [21].	11
Figure 9	Accelerated stress test results of (a) Pt/TiO ₂ over 200 h and (b) Pt/C over 80 h [39].	13
Figure 10	Screening the activity and stability using DFT calculation. The horizontal axis is the heat formation energy which can be related to stability. The vertical axis is the bonding energy which is an indicator of activity [41].	15
Figure 11	(a) Bright field image of Pt/Sc ₂ O ₃ /C. the light grey area is free of C; and (b) the EDAX mapping of the squared area.	19
Figure 12	Dark field and bright field images of (a) the voids on the Sc ₂ O ₃ nanosheets; (b) adjacent area of the nanosheets marked in red and carbon support marked in green; and (c) free standing nanosheets.	20

Figure 13	TEM images of (a) Pt nanoparticles obtained without Sc precursor; (b) Pt supported on CeO nanosheets synthesized via similar method; and (c) EDAX spectrum showing the presence of Ce_xO_y	21
Figure 14	(a) CV of Pt/Sc ₂ O ₃ /C catalyst with clear Pt features; and (b) ORR polarization curves of Pt/Sc ₂ O ₃ /C with and without IR correction.	22
Figure 15	(a) Specific activity and (b) mass activity comparisons of Pt/C and Pt/Sc ₂ O ₃ /C at the beginning and after 6,000 cycles of test.....	23
Figure 16	XPS measurement comparison of Pt/C and Pt/Sc ₂ O ₃ /C.....	23
Figure 17	ECSA loss during durability test for Pt/C and Pt/Sc ₂ O ₃ /C.....	24
Figure 18	(a) TEM image of free Au particles without carbon support; (b) histogram of Au particles; and (c) EDAX of the particles.	29
Figure 19	CV of Au/C in 0.1 M KOH with different upper potential, the reduction peak size is proportional to the potential upper limit.	30
Figure 20	(a) ORR polarization curves at different rotation speed with sweeping rate 50 mV/s; (b) Levich-Koutecky Plots for the ORR on Au at various potentials extracted from data in (a); current density normalized to the geometric electrode area.	31
Figure 21	ORR polarization curves of Au/C and Pt/C both at the beginning (solid line) and at the end (dash line) of the durability test with ECSA loss comparison inset.....	32

ABSTRACT

The sluggish oxygen reduction reaction (ORR) kinetics remains the critical technical barrier to fuel cell technology commercialization. In this thesis, the mechanisms, critical problems, and current research activities are first discussed. Then, with insights gained from literature, two different types of catalysts are explored for the electrochemical reduction of oxygen.

Pt/Sc₂O₃ was synthesized using wet chemistry approach. Analysis under high-resolution transmission electron microscopy (HRTEM) revealed the unique nanosheet structure of the Sc₂O₃. Physical and chemical properties of the catalyst were examined including the morphology, particle size, and chemical bonding strength. Rotating disk electrode (RDE) measurement was carried out to evaluate the activity of the catalyst in an acidic environment. The observed catalyst activity is three times higher than the benchmark Pt/C. Furthermore, durability tests showed the electrochemical surface area (ECSA) losses of the catalyst is only one third of that of Pt/C after 30,000-cycles of durability test. The second catalyst explored is designed for hydroxide exchange membrane fuel cells. Specifically, a platinum-free nano-Au supported on C was also produced under mild synthesis conditions. Ozone treatment was used to remove the surfactant on the surface of the particle. The activity was determined via RDE in alkaline medium. The specific activity of Au/C is remarkably approaching that of the Pt/C. In addition, the Au/C loses 9 % of the initial surface while the Pt/C has a loss of 40 % after a modified stressful durability test. The results from this study provide useful information and guidance to the research of future catalysts.

Chapter 1

INTRODUCTION

With the worldwide depletion of fossil fuels and the continually growing energy demand of human society, finding sustainable and reliable next-generation power source has been one of the critical topics of the past century. Fuel cells have drawn great attention as an environmentally friendly and high-efficiency electrochemical devices [1]. Fuel cells are generally categorized by their working electrolyte: acid fuel cell, alkaline fuel cell, solid oxide fuel cell and so on. Among all of these, the polymer electrolyte membrane fuel cell has been the most extensively studied. It has the advantages of portability, mild operating conditions and compatibility with a variety of fuels [2]. Polymer electrolyte membrane fuel cells can be further divided into two types, proton exchange membrane fuel cells (PEMFCs) and hydroxide exchange membrane fuel cells (HEMFCs) depending on the type of membrane employed.

Figure 1 shows the structure and chemistry of operating PEMFC using hydrogen as fuel and oxygen as oxidant. On the anode side, hydrogen is oxidized to produce protons and electrons. While the protons are transferred through the membrane, the electrons go through the external circuit to produce electricity. Upon meeting again at the cathode, they will spontaneously react with oxygen to produce water in the presence of a catalyst. For the HEMFC, the mechanism is similar, except that the transferred ion is hydroxide rather than proton.

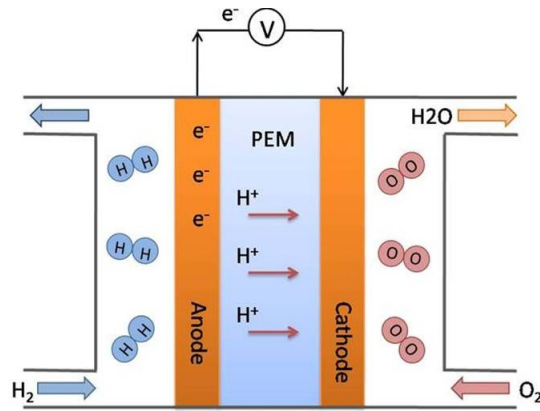


Figure 1 Scheme of PEMFC using hydrogen as fuel and oxygen as oxidant.

The commercialization of PEMFC has been inhibited by the high material cost associated mainly with the Pt catalyst required for both the anodic hydrogen oxidation reaction (HOR) and cathodic oxygen reduction reaction (ORR). For PEMFCs, Pt is so far the only practical catalyst due to the device's highly oxidative and acidic environment during operation. Between the two half-cell reactions, the ORR is a bigger concern since its large over-potential (300~400) severely limits performance [3]. So far, the commercial catalyst of 2 ~5 nm Pt nanoparticles supported on carbon still suffers from the poor activity and durability.

HEMFC has a much shorter history than PEMFC. The switch from PEM to HEM makes the utilization of non-Pt or even non-precious-metal catalysts possible. Recently, the research of high performance HEMs is advancing rapidly [4-6]. Nonetheless, finding a cheaper and more active catalyst for the device is still a big concern. Studies show that even with the best catalyst (Pt), the HOR in HEMFC has a much higher over-potential than in PEMFC. While there has been some success in

non-precious metals in alkaline fuel cells for ORR [7-9], such study in HEMFC is still rare.

With the growing interest in both PEMFCs and HEMFCs, novel catalysts with better activity and durability are in great demand.

Chapter 2

RESEARCH BACKGROUND

ORR Mechanism

The oxygen reduction reaction on a metal surface is a complex heterogeneous catalytic reaction which involves several elementary steps. Two general reaction mechanisms have been proposed, illustrated schematically in Figure 2.

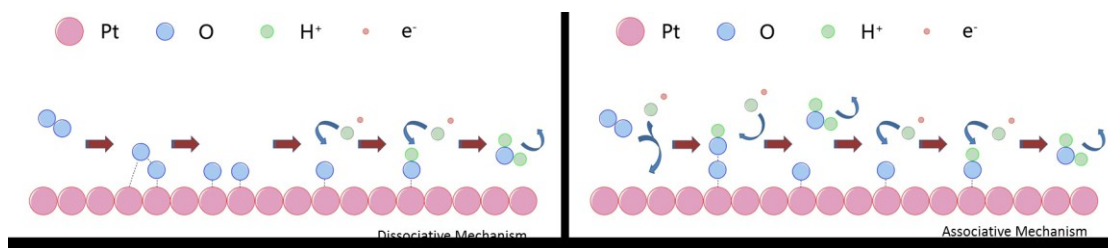


Figure 2 ORR mechanisms of dissociative and associative mechanism.

Regardless of the details, it consists broadly of adsorption, reaction and desorption steps. The reactivity of the metal surface is controlled by the activation energy of the rate determining step, which in most cases is either the adsorption or desorption step. According to study of T. Bligaard [10], the activation energy is proportional to the bonding energy of metal and adsorbate which reflects the interaction strength between them. This is a very significant result in heterogeneous

catalytic studies because it provides the relationship between a catalyst's intrinsic properties and reactivity.

More specifically, weak bonding corresponds to the adsorption-limited case, in which large activation energy is required for the adsorbates to bond with the catalyst surface. Conversely, strong bonding corresponds to the desorption-limited case, in which the surface of the catalyst will be blocked by the strongly bonded reaction intermediate and the active surface sites will continuously decrease with the accumulation of the intermediates [11]. Accordingly, a good catalyst surface must be reactive enough to form the bond and noble enough to release the product [12].

ORR Activity on Pt Surface

Figure 3 [13] shows the free energy change of oxygen reduction reaction on Pt surface with different oxygen coverage under different potentials. The three black lines compare different potential. At $U=0$ V, the free energy change of all steps is downhill, indicating the forward reactions are all favorable. At higher potential, the difference between the reactants and products becomes smaller, so driving force for the forward reaction is much less. At $U=1.23$ V, which is the standard reduction potential for oxygen, the last two steps become even more difficult showing an uphill free energy change. The blue line of oxygen coverage of 0.5 illustrates that at higher adsorbate coverage, the Pt surface is less active for both the adsorption and proton transfer steps. This graph suggests that the Pt is bonding too strongly with the adsorbed oxygen atom, making the following proton transfer step unfavorable. Similar study of ORR on all other metals can be done and the results will provide a rough screening for oxygen reduction catalysts.

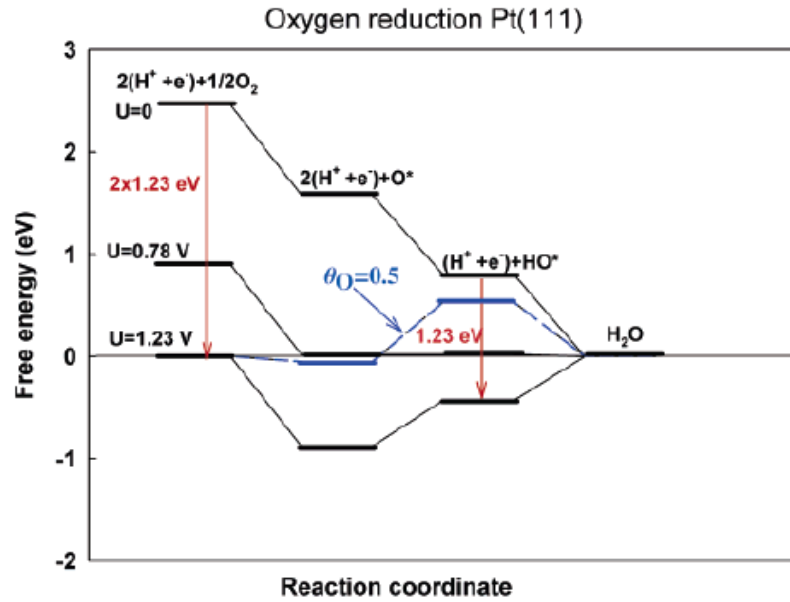


Figure 3 Free energy chart of oxygen reduction reaction on Pt surface of dissociative reaction mechanism [13].

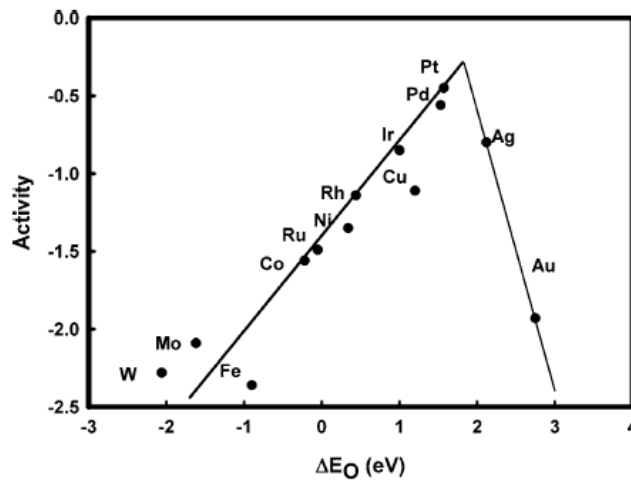


Figure 4 Volcano plot of ORR activity on different metal surfaces [13].

In previous work, J. Nørskov and co-workers plotted the ORR activity of different metal surfaces against the oxygen bonding energy [13, 14]. The plot has a

volcano shape as shown in Figure 4, with the strongly bonding elements on the left side and the weakly bonding elements on the right side. Clearly, Pt is the closest to the optimum and better activity is expected if we can tune the Pt-O bond to be weaker.

While other metals (silver, palladium, copper and so on) also show acceptable activity, their strong tendency to dissolve in acid makes them less competitive in practical applications [15].

Stability of Pt for ORR

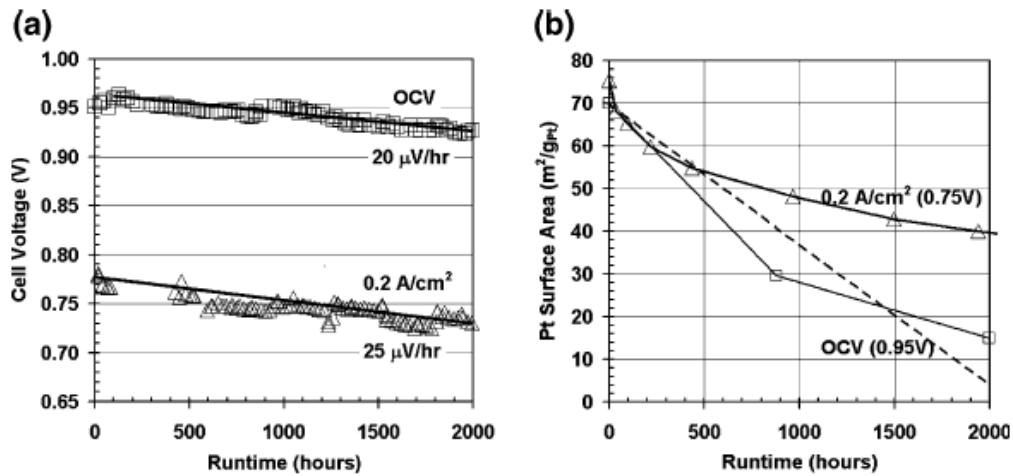


Figure 5 Cell voltage (a) and Pt electrochemical surface area (b) as a function of short-stack run time. Operating condition: Hydrogen/air stoichiometric flow is 2/2, under 80 °C, 150 kPa_{abs}, 100% RH [16].

The conventional PEMFC catalyst consists of 2~5 nm Pt nanoparticles dispersed on a high surface area carbon support. The particle size maximizes utilization of the Pt surface. However, the electrochemically active surface greatly diminishes during fuel cell operation. Figure 5 [16] shows clearly the potential and Pt

surface area losses as a function of time. A significant part of the losses can be attributed to the slow cathodic kinetics.

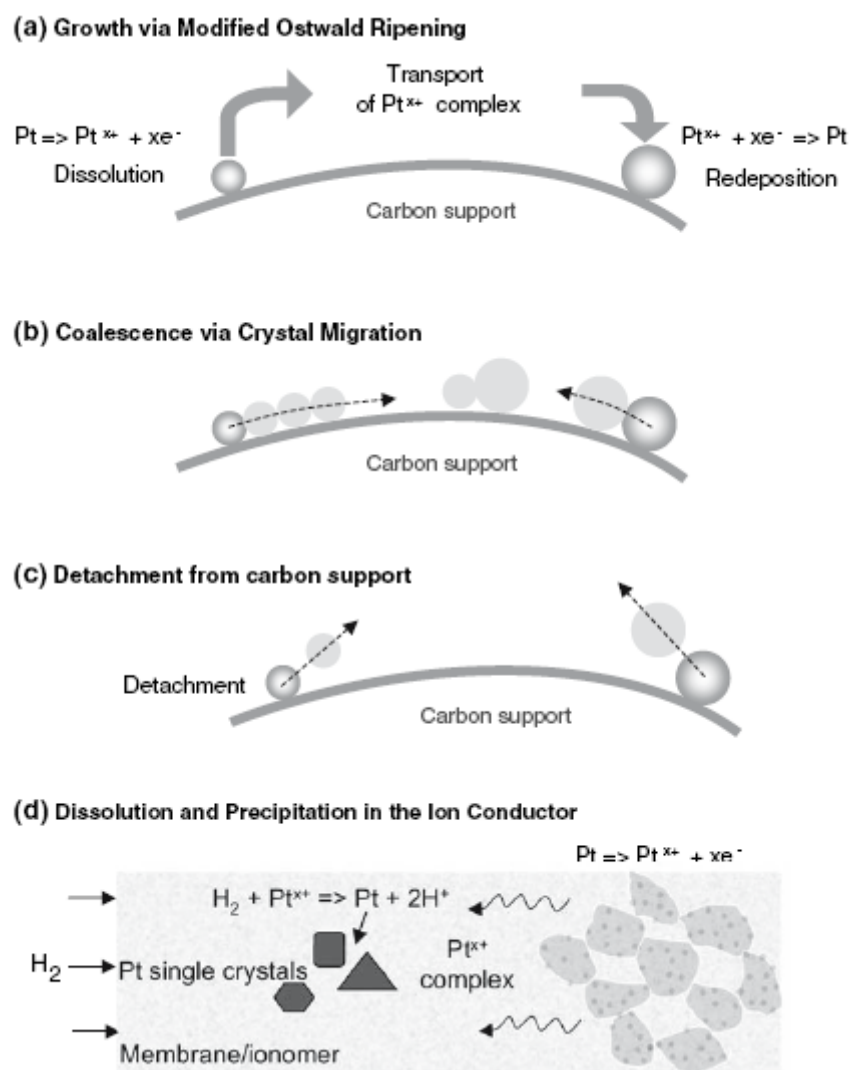


Figure 6 Proposed mechanisms of instability of Pt particles in low temperature fuel cells [17].

In general, four main mechanisms for Pt degradation have been proposed in previous literature [17, 18] as shown in Figure 6 [17]. Ostwald ripening is a thermodynamically driven process, in which smaller Pt particles will dissolve and re-deposited on larger particles. In this way, the particles grow larger at the expense of high-surface-area small particles. The second mechanism describes the movement of Pt particles on the carbon support and the coalescence when particles meet. In the third mechanism, detachment of particles from carbon support becomes considerable during start-up and shut-down due to severe carbon corrosion. The last mechanism mainly refers to Pt loss in the catalyst layer due to the re-deposition in the ion conductor and membrane layer.

With the help of the advanced microscopy, a recent study revealed the structure evolution during the degradation of Pt (and PtM) nanoparticles at the atomic level [19-22]. By using an indexed gold grid, they were able to take images of exactly the same part of the sample. We can clearly observe the movement and coalescence of the particles on the carbon surface in Figure 7 (c), (d) and (e)[22].

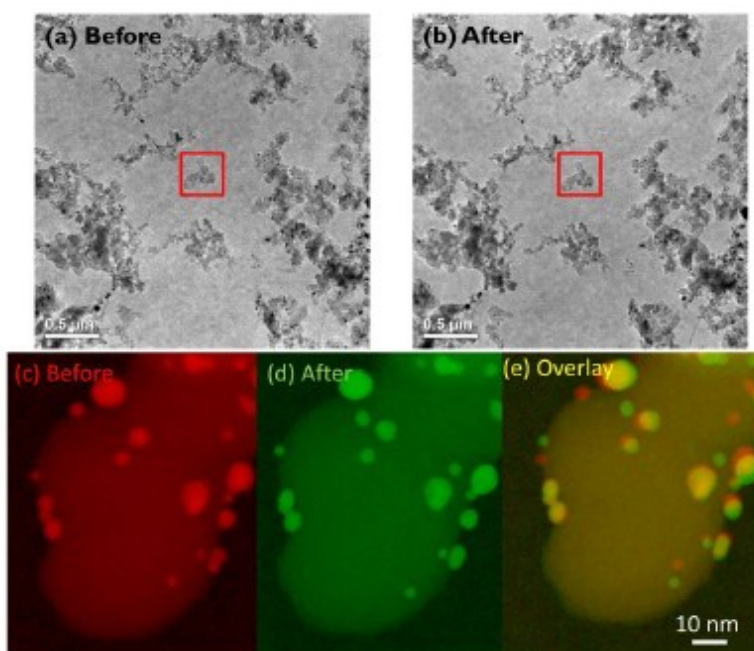


Figure 7 Microscopic images of PtCo/C sample with low resolution (a) before (b) after the durability test and with high resolution (c) before, (d) after and (e) overlay of the two [22].

In follow-up study [21], the authors were able to take hundreds of images of PtCo nanoparticles of the same sample. As mentioned previously, Co is not stable in acidic environments and will be dissolved. As a result, a core-shell structure is produced with a PtCo core and Pt shell. Two different types of core-shell structures showed up in the elemental mapping images in Figure 8 [21]: single-core and multi-core. While the single-core particles are a result of Ostwald ripening, the multi-cores can only be generated from the coalescence of particles. In this way, the authors demonstrated the significant contribution of Ostwald ripening and particle coalescence to the degradation of the active Pt surface area.

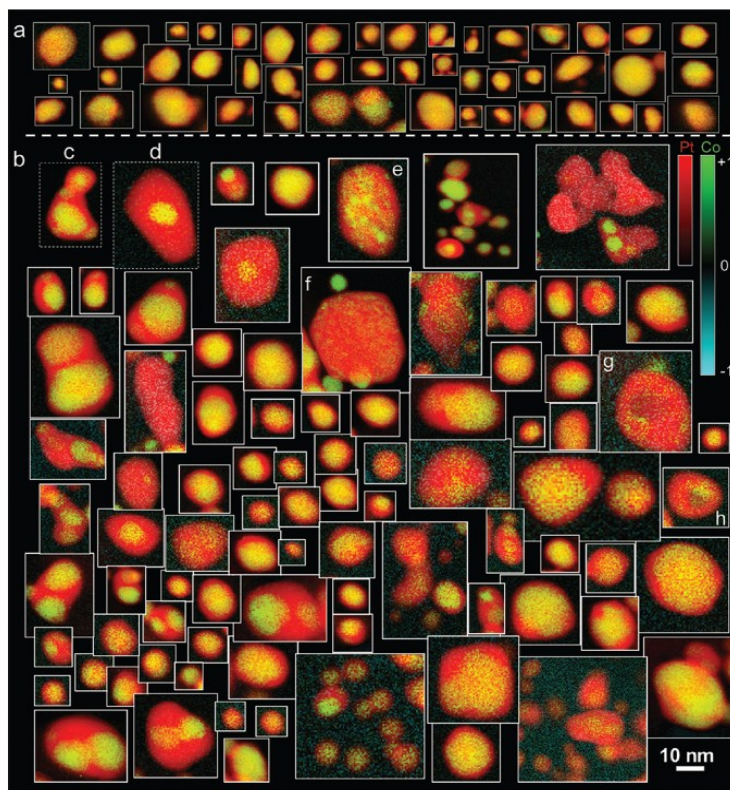


Figure 8 Hundreds of elemental mapping images of the PtCo particles, (a) before and (b) after the durability test; (c) and (d) presents an example of multi-core and single-core particle respectively [21].

Selective Research Activities

Research to understand reaction/degradation mechanisms and explore new catalysts has been carried out for the past several decades. Nowadays researchers mainly focus on three directions: improving activity, increase Pt utilization and enhancing durability of the catalyst.

As an effective way to tune the activity of Pt, alloying is one of the most extensively studied strategies. Previous studies demonstrated a substantial improvement in specific activity of PtM [23-25] due to the electronic structure tuning from the second metal, such as Co, Fe, or Ni. A general trend which can be seen in

both experimental and computational modeling studies is that when Pt is alloyed (or incorporated into a layered structure) with elements that bond strongly with oxygen, like the ones on the left side of the volcano plot, the bonding between Pt and oxygen weakens. Pt-based alloys can not only improve the intrinsic activity of Pt, but also reduce the usage of Pt compared to particles of similar size.

The mechanism of ORR on Pt alloys has been studied for more than 20 years. Some researchers attributed higher activity on bulk PtCr alloys to surface roughening [26]. Others attributed the activity to particle termination with particular vicinal planes on dispersed catalyst surfaces [27]. In a paper published 1983 [28], the authors investigated the relationship between interatomic distance and catalytic activity for Pt alloys in phosphoric acid. They used XRD to determine the nearest neighbor distance of 10 different Pt alloys. A linear relation curve was observed upon plotting the activity against nearest neighbor distance. Still others researchers attributed the activity to the electronic tuning from the ligand effect (such as d-band vacancy) and the strain effect caused by introducing other metal atoms into the Pt lattice [29, 30].

Despite their high activity, the stability of alloy catalysts is still a concern. Studies [31] show that, since the second metal is much less stable than Pt, over long-term fuel cell operation, the second metal will leach out, leading to a dramatic change in catalyst composition and activity. The final structure of catalyst usually consists of a skeleton Pt skin [32, 33] which is vulnerable to dissolution [34].

Another strategy to reduce Pt usage is to construct materials with novel nano-structure, for instance, Pt monolayers supported on other metals. Adzic and co-workers successfully generated Pt monolayer supported on both single-crystal [35] and nanoparticulate metal surfaces [36, 37]. Results showed that when Pt is supported

on Pd, the activity can be improved. Due to the low amount of Pt being used, the mass activity can be improved considerably. However, the stability is still under debate.

Theoretical studies [15, 38] claim that the monolayer structure is not thermodynamically stable: the top layer will diffuse into the base metal to form a solid solution.

Two strategies have been explored to improve durability. One is to replace the carbon support with other materials, such as TiO_2 [39]. As shown in Figure 9, with comparable initial membrane electrode assembly (MEA) performance, the Pt/ TiO_2 has a much longer lifetime than Pt/C. The other method is to construct free-standing Pt catalyst without C support. As reported by S. Alia [40], the Pt nanotube degrades much less than Pt/C after a 30,000 cycle durability test.

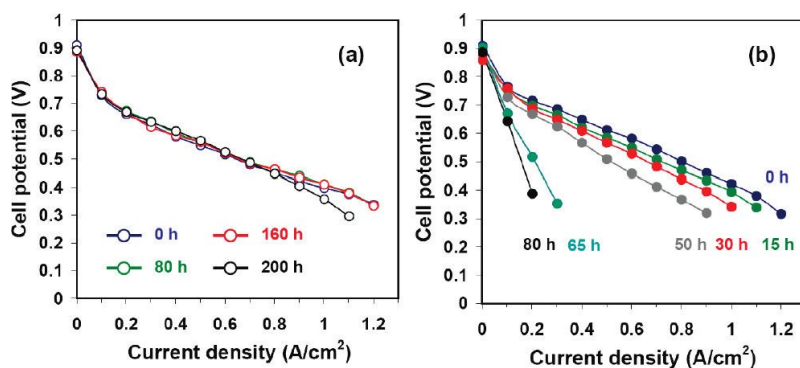


Figure 9 Accelerated stress test results of (a) Pt/ TiO_2 over 200 h and (b) Pt/C over 80 h [39].

Other studies concerning non-precious metal catalyst development are outside the scope of this thesis.

Chapter 3

CATALYST OF PT SUPPORTED ON SCANDIUM OXIDE NANOSHEETS FOR PEMFC

Background

Most of the early studies of the Pt alloy catalysts have been limited to late transition metal (or group VIIB metals), such as Ni, Co, Fe group. . It is only recently that studies have incorporated the early transition metals and rare earth, transition metals. In 2009, J. Greeley [41] published results from density functional theory (DFT) calculations for various PtM systems. Of particular interest were the resulting predictions for Pt(Pd)₃M and Pt(Pd)M systems. Specifically, relationships between bonding energy and predicted activity, and alloy heat formation energy and resulting stability were discussed. The useful result is summarized in Figure 10 [41]. The calculations suggest that PtY and PtSc are two promising candidates for PEMFC catalysts, due to their suitable bond energy and predicted.

Inspired by this finding, Dr. Chorkendorff and others have extended the study to other rare metals, such as Gd, Hf and Zr [42-46]. In these studies, the authors have reported activity, stability, and durability of various synthesized catalysts. For example, durability tests of bulk Pt₅Gd show nearly no decreases in activity after 30,000 cycles.

Given the favorable results of the previously synthesized materials above, and the potentially good candidates PtY and PtSc as suggested by Figure 10, synthesis of

Pt with early transition metals are a promising next step. However, metals such as Sc, Y, Hf, and Gd have very negative reduction potential, which indicate difficulty in forming alloys. Up to now, no studies have been reported of these materials in nano-scale.

In the following section, the author summarized her study on synthesis and characterization of Pt/Sc₂O₃/C composite catalysts. The interesting observations and results will be discussed in details as well.

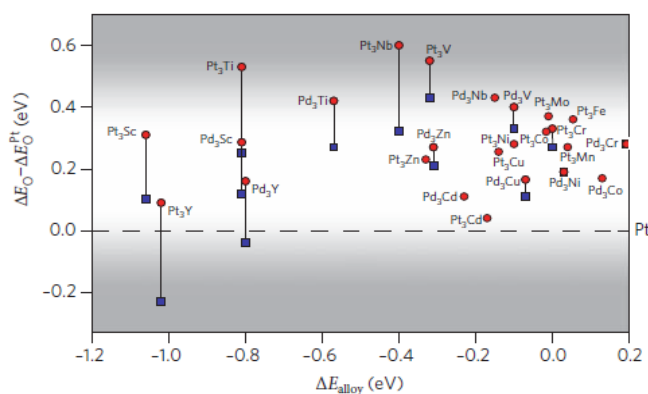


Figure 10 Screening the activity and stability using DFT calculation. The horizontal axis is the heat formation energy which can be related to stability. The vertical axis is the bonding energy which is an indicator of activity [41].

Experiment

Synthesis of Pt/Sc₂O₃/C Catalyst

Pt supported on Sc₂O₃ was prepared by an organic solvothermal method. In a typical synthesis, 68 mg scandium acetylacetonate (Alfa-aesar) and 129 mg 1,2-hexanediol (Sigma-Aldrich) were dissolved in 20 mL diphenyl ether (Sigma-Aldrich) in the presence of 1 mL oleic acid (Sigma-Aldrich) and 1 mL oleylamine

(Sigma-Aldrich). The mixture was heated to 80 °C, under Ar atmosphere, to get a clear solution before being raised to 240 °C. Next, 30 mg platinum acetylacetonate (Sigma-Aldrich) in 0.5 mL dichlorobenzene (Sigma-Aldrich) was injected into the solution, which immediately turned dark brown, indicating the formation of metal nuclei. The reaction was maintained at 240 °C for 1 h before cooling down to room temperature for collection.

Post-treatment

The Pt/Sc₂O₃ catalyst was loaded onto high surface area carbon support before washing. Typically, 15 mg Ketjen carbon black was dispersed in 10 to 15 mL isopropanol. The as-synthesized catalyst was added to the mixture under vigorous stirring at 80 °C. After 30 min, the mixture was transferred to an ultrasound bath for another 30 min mixing. The product was collected by centrifuge and washed with hexane and ethanol 3 times.

High temperature annealing was done to remove any residual organic surfactant. Under these conditions, the catalyst has been shown to retain its particle size and composition [47]. In this synthesis, the carbon supported catalyst was transferred to a ceramic boat and placed in a tube furnace. The catalyst was then annealed at 650 K or 700 K for 30 min in a H₂ and Ar mixture prior to further characterizations.

Thermal Gravimetric Analysis

The carbon to metal loading ratio was obtained from a thermal gravimetric analyzer. For each test, approximately 2 mg of catalyst was loaded in an alumina

crucible. The temperature was raised to 900 °C under oxygen to burn off all the carbon. The remaining residue is considered as carbon-free.

Transmission Electron Microscopy

TEM was carried out using JEM-2010 FX in the W.M. Keck Electron Microscopy Facility Center at the University of Delaware. To prepare the sample suspension for TEM, a small amount of dry powder was dispersed in methanol and sonicated. Afterward, the Lacey Carbon copper grid was coated with a drop of the sample suspension and dried thoroughly before being loaded into the TEM chamber. The dark field images and Z-contrast images were obtained using JEOL 2200FS STEM with a CEOS probe-corrector from Oak Ridge National Laboratory. The STEM instrument is also equipped with a Bruker-AXS silicon drift detector for recording EDS maps, which investigate the composition of the catalyst.

Surface Composition and Binding Strength

Surface composition was obtained with a Phi 5600 X-ray photoelectron spectroscopy (XPS) system equipped with a multi-channel hemispherical analyzer and Al anode X-ray source. The XPS was calibrated using binding energies of the primary peaks from Au, Ag, and Cu reference samples. Samples were prepared by pressing the powder into In foil before mounting on a sample holder. The Pt/Sc atomic ratio was determined from the Pt 4f and Sc 2p photoelectron peaks.

Electro-chemical Measurements

Rotating disk electrode (RDE) measurements were used to evaluate the activity of the catalyst. First, catalyst powder was dispersed in ultrapure DI water. 20 μ L of the suspension was dropped onto a glassy carbon electrode and dried in air at room

temperature to form a uniform thin film. Later, 10 μL of a 0.005% Nafion in ethanol solution was dropped on top of the electrode as a conducting binder. The loading on the electrode was adjusted to 10 to 20 $\mu\text{g Pt}/\text{cm}^2$ of electrode surface for both the synthesized catalyst and the commercial Pt/C. The electrochemical test was conducted in a jacketed electrochemical glass cell. A saturated Calomel electrode and a Pt wire were used as reference and counter electrodes. All measurements were carried out in 0.1 M HClO_4 at room temperature (RT). The electrochemical surface area (ECSA) was obtained from the Pt hydrogen adsorption and desorption region of the cyclic voltammogram. This involved integration to find the total charge, and then dividing the total charge by the charge density of Pt [48]. The ORR catalytic activity was obtained from the ORR polarization curve. The current at 0.9 V vs. RHE was taken from the curve using a sweep rate of 20 mV/s. Durability tests were carried out by cycling the potential from 0.6 V to 1.1 V vs. RHE for 30,000 cycles at RT with a sweep rate 50 mV/s. ECSA measurements were taken at the 6,000th, 12,000th, 18,000th, 24,000th and 30,000th cycle.

Results and Discussions

Morphology and Growth Mechanism of Pt/Sc₂O₃/C

Solvo-thermal method has been applied to successfully produce PtM (M=late transition metals) alloy nano-crystals before [49-51]. Typically, the co-reduction of Pt and Ni, Co or Fe will produce uniform PtM nanocrystals. But in the case of Pt-Sc system, the product is quite different. Figure 11 (b) is the EDAX mapping image corresponding to the squared region of (a) the bright field image. The Pt signal is represented by red dots while the Sc signal is represented by green. A sheet-like

structure with strong Sc signal in the area is observed. From the elemental analysis, the strong oxygen peak confirms the composite of Sc_2O_3 . Rather than forming uniform alloy nanocrystals, scandium oxide nanosheets were produced and serve as another support for Pt nanoparticle dispersion. In Figure 12, there are three sets of bright field and dark field images revealing the structure of Sc_2O_3 nanosheets explicitly. The oxide nanosheets are not uniform in thickness. In Figure 12 (a) and (b), the voids and differences in thickness of each nanosheet can be seen from the contrast. Under low magnification, the nanosheets have similar morphology and cannot be clearly distinguishable from carbon. However, at high magnification (d), the lattice of the Sc_2O_3 (separated by red line) can be seen, compared to the amorphous carbon (separated by green line). There also exist free standing Sc_2O_3 nanosheets in the sample, which are fully unattached to any carbon support as shown in Figure 12 (e) and (f).

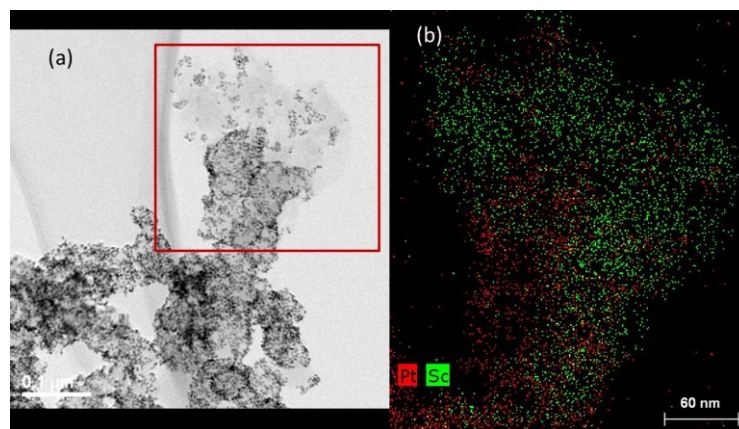


Figure 11 (a) Bright field image of Pt/ Sc_2O_3 /C. the light grey area is free of C; and (b) the EDAX mapping of the squared area.

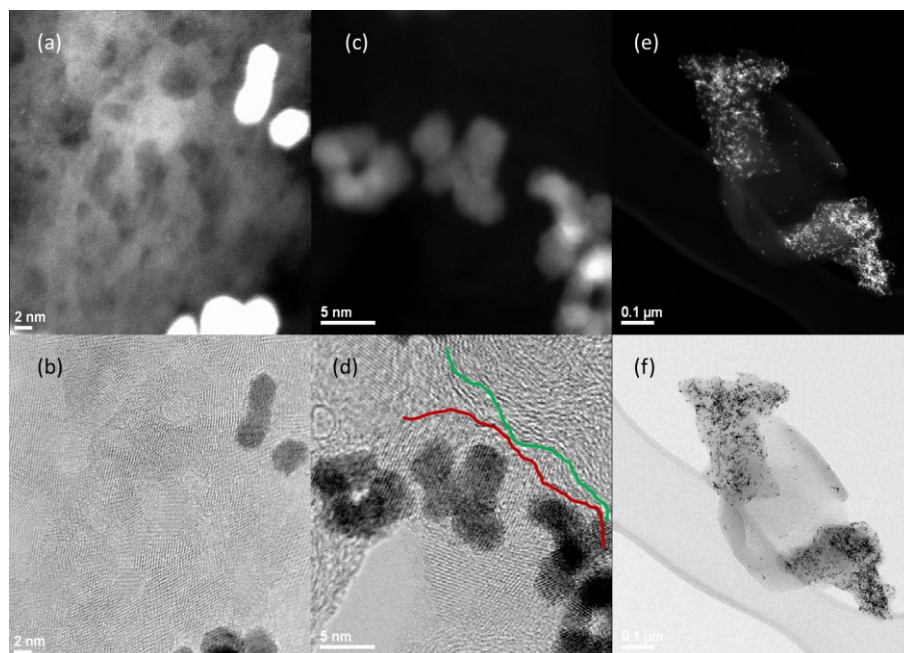


Figure 12 Dark field and bright field images of (a) the voids on the Sc_2O_3 nanosheets; (b) adjacent area of the nanosheets marked in red and carbon support marked in green; and (c) free standing nanosheets.

Studies were carried out to determine the effect of Sc on catalyst formation. The first study involved a control synthesis without Sc precursor. Results showed that Sc_2O_3 formation plays an essential role in separating the Pt particles and preventing them from aggregating into larger entities. As illustrated in Figure 13 (a), the Pt particle size is much larger without Sc precursor, compared to that of the original recipe with Sc. When the Sc precursor was substituted with a Ce precursor, which has similar chemical properties as Sc, interestingly, the nanosheet structure was again generated as shown in Figure 13 (b). The EDAX indicated the presence of Ce_xO_y in the light grey area of the nanosheets.

This simple method to produce metal oxide supported Pt catalyst has never been reported before. Since elements like Sc and Ce are chemically too active to be reduced to their zero valences, they are more likely to form oxides during the synthesis.

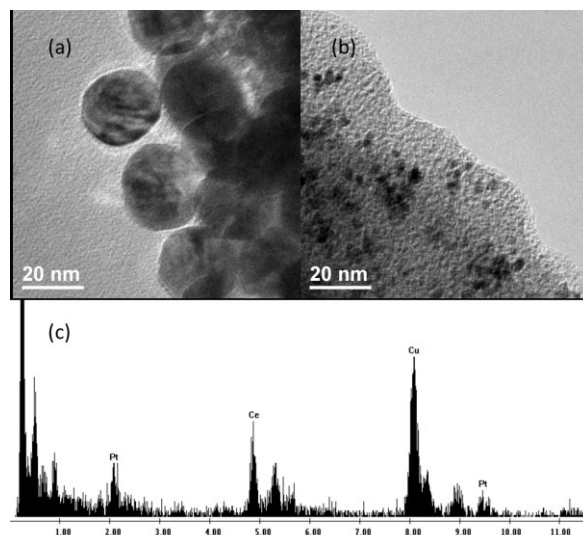


Figure 13 TEM images of (a) Pt nanoparticles obtained without Sc precursor; (b) Pt supported on CeO nanosheets synthesized via similar method; and (c) EDAX spectrum showing the presence of Ce_xO_y .

ORR Activity and XPS

Since Sc_2O_3 is not stable in the electrochemical testing environment, the nanosheets will be dissolved eventually. Pt/ Sc_2O_3 /C catalyst exhibits typical Pt features in the CV as shown in Figure 14 (a). The ORR polarization curve was obtained at room temperature with sweeping rate 20 mV/s. Both the original and IR-corrected curves are shown in Figure 14 (b). The significant deviation between original and IR-corrected curves suggests that the resistance from the support and/or conducting binder cannot be ignored. For the sake of comparison, the commercial catalyst, 20% Pt/C provided by EC-lab, was also tested. The results for both specific

activity and mass activity are summarized in Figure 15. The lab-synthesized Pt/Sc₂O₃/C catalyst exhibits about 3 times higher specific activity, which already surpasses the DOE's target for 2015 (marked by the blue dash line). Slight improvements in specific activity were observed for both of the catalyst in the longer run (6000 cycles), due to growth of Pt nanoparticles. The initial mass activity of Pt/Sc₂O₃/C is 0.42 mA cm⁻², which is very close to the DOE target of 0.44 mA cm⁻². Surprisingly, after 6000 cycles, the Pt/Sc₂O₃/C catalyst showed improvement in mass activity of about 20 %. This can be explained by the “peel off” process of the catalyst. During the synthesis, some of the Pt particles will be covered by the Sc₂O₃ nanosheets. And these Pt particles do not provide active surface until the nanosheets are leached away by the acid gradually. The author believes that this “peel off” process will protect the Pt from dissolution at the early age of the test and slow down the degradation process.

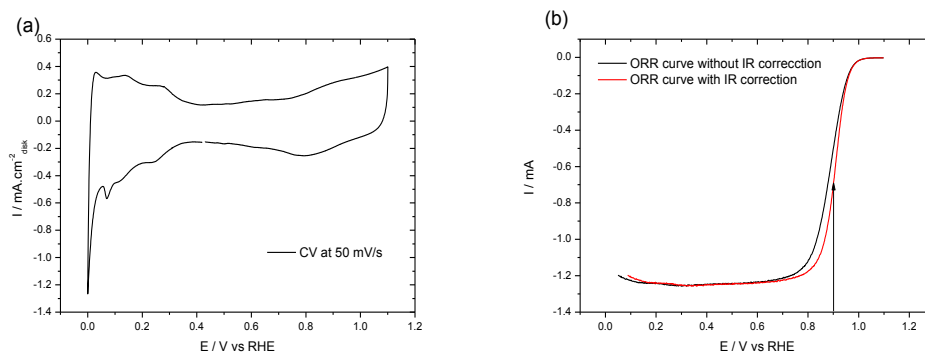


Figure 14 (a) CV of Pt/Sc₂O₃/C catalyst with clear Pt features; and (b) ORR polarization curves of Pt/Sc₂O₃/C with and without IR correction.

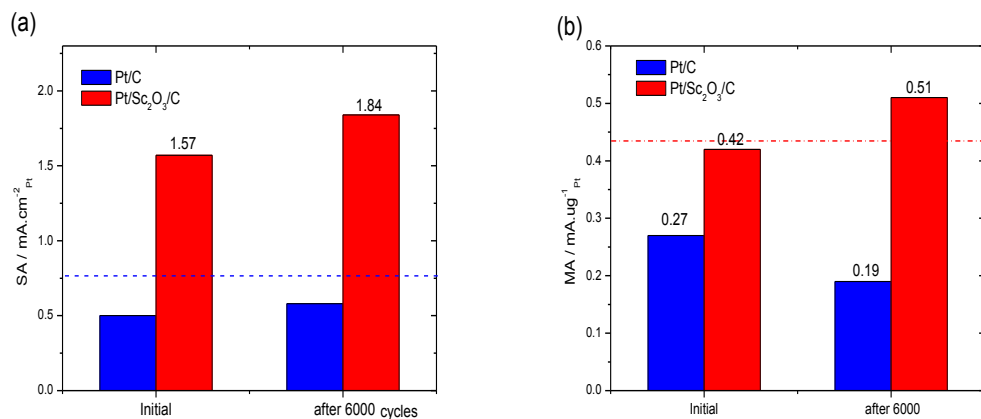


Figure 15 (a) Specific activity and (b) mass activity comparisons of Pt/C and Pt/Sc₂O₃/C at the beginning and after 6,000 cycles of test.

Figure 16 is the XPS results for Pt/C and Pt/Sc₂O₃/C. The original signal is deconvoluted into Pt and Pt oxide peak. With much smaller Pt oxide formation in the Pt/Sc₂O₃/C, the binding energy is weakened and subsequently, the specific activity is improved compared to that of Pt/C. This result further confirms a beneficial tuning effect is indeed introduced by the Sc₂O₃ support.

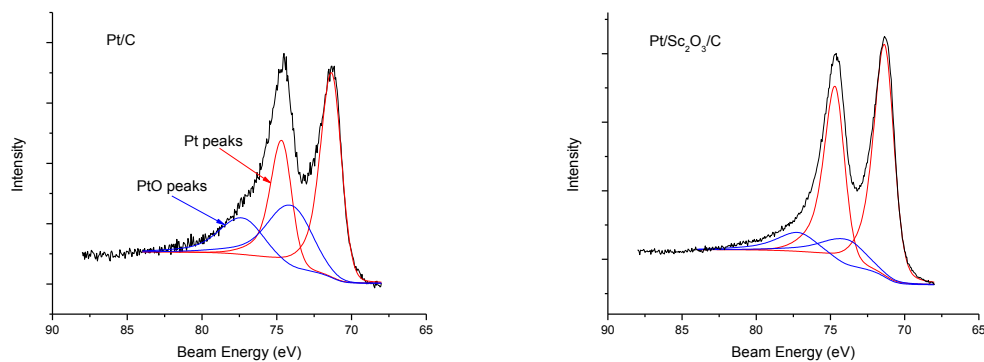


Figure 16 XPS measurement comparison of Pt/C and Pt/Sc₂O₃/C

ORR Durability of Pt/Sc₂O₃/C

A durability test was carried out over 30,000 cycles, with the potential ranging from 0.6 to 1.1 V, which is slightly larger than reported in literatures [40, 52]. Larger potentials correspond to harsher environments for durability testing. Figure 17 summarized the ECSA loss during the durability test. As proposed previously, the “peel off” process of Pt/Sc₂O₃/C first results in an increase in the ECSA. By the end of 30,000 cycles, the ECSA gradually decreases to 77 % of the initial surface area. In contrast, the commercial Pt/C sample lost about 40 % of the surface area within the first 6,000 cycles, due strong dissolution and coalescence of tiny Pt particles. Only one quarter of the initial surface area of Pt/C remains after the durability test.

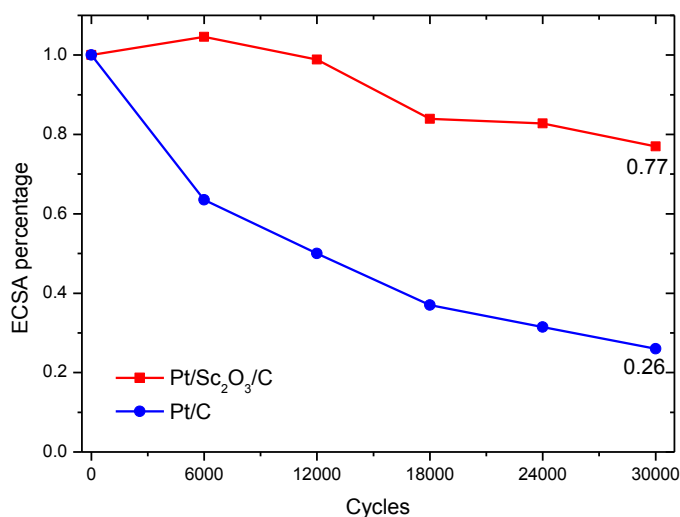


Figure 17 ECSA loss during durability test for Pt/C and Pt/Sc₂O₃/C.

Summary

For the first time, metal oxide supported Pt catalyst (Pt/Sc₂O₃/C) has been synthesized via a simple one pot reaction. The morphology and growth mechanism of

these oxide nanosheets have been discussed. The interaction between Pt nanoparticles and Sc_2O_3 nanosheets result in a beneficial tuning effect on catalytic reaction of oxygen. The lab-made catalyst exhibits a ORR activity that is three times as high as Pt/C. It also has much slower degradation rate. At the end of a 30,000 cycle durability test, about 80 % of the electrochemical surface area remains. This is very promising for practical application.

Chapter 4

STUDY OF NANO-GOLD PARTICLES FOR ORR OF HEMFCS

Background

Many studies have looked at designing catalysts with the intention of minimizing the use of expensive and limited Pt. However, the ideal solution may be to eliminate its use entirely. Efforts on non-Pt catalysts are currently a hot topic. For example, Au has been looked at as an alternative catalyst, since it offers unique properties. Compared to Pt, bulk Au has very poor catalytic performance because of its less active surface. At the nanoscale, however, Au metal becomes quite reactive. Studies showed small particles of Au to have surprisingly high activity and selectivity for CO oxidation, as well as other oxidation reactions involving small molecules [53]. Typically, the mechanism for oxygen reduction using a Pt surface occurs via a 4-electron transfer pathway. In contrast, on bulk Au, oxygen reduction generally goes through a 2-electron transfer mechanism due to the weak binding between the Au surface and its reaction intermediates [54]. As a result, the efficiency for energy conversion is lower, as evidenced by its decreased activity compared to Pt. When the particle size decreases, there is an increase in the fraction of atoms with low coordination number and high tendency for reaction. Thus, the activity and even the mechanism of nanoscale materials can be very different from that of the bulk. Therefore, there have been several studies about the size and facet dependence of Au for the reduction of oxygen [54-56].

Even under similar particle size, however, studies have shown that the activity of Au is quite dependent on the particular synthesis method, preparation procedure, and/or treatment process [54-58]. Furthermore, the study of the stability of Au catalysts for ORR is quite lacking. In this work, the author did a systematic study of synthesis and characterization of ultra-small gold particles. Both the initial activity and stability have been discussed and compared to standard Pt/C. The result will provide useful information for further developing Au-based catalyst.

Experiment

Catalyst Preparation

The synthesis procedure can be found elsewhere [59]. In a typical synthesis of ultra-small gold nanoparticles, 0.1 g $\text{HAuCl}_4 \cdot 3\text{H}_2\text{O}$ (Alfa) was dissolved in 10 mL tetralin (Sigma-Aldrich) and 10 mL oleylamine (Sigma-Aldrich), all in a three-neck round-bottom flask. The solution was stirred under Ar for 10 min at 30 °C. After obtaining a clear solution, 0.5 mmol TBAB (Tetra-n-butylammonium bromide, Sigma-Aldrich) dissolved in 1 ml tetralin and 1 ml oleylamine was injected into the reactor. The solution color quickly changed from transparent to dark brown, indicating the formation of Au nuclei. Growth of the nanoparticles was carried out for 1 h before washing with hexane and ethanol.

To load the particles on carbon support, 20 mg Ketjen carbon was dispersed in 50 mL isopropanol. The hexane suspension with Au particles was added dropwise into the carbon suspension under vigorous stirring. After sonicating for 30 min, the carbon supported sample was washed with isopropanol for three times before further characterization.

Transmission Electron Microscopy

The size of gold nanoparticles was determined using JEM-2010 F TEM in the W.M. Keck Electron Microscopy Facility Center at the University of Delaware. In preparing the samples for TEM, the carbon loaded sample was dispersed in isopropanol and sonicated to form dilute suspension. Then the Lacey Carbon copper grid was coated with a drop of the mixture and dried thoroughly before loaded into the TEM chamber.

Electrode Preparation

The electrochemical measurement was carried out similarly as described in Chapter 3, aside from the preparation of the working electrode. To prepare the Au electrode, the carbon supported catalyst was dispersed in isopropanol at a concentration of 0.3 mg/mL. After sonication, 5 μ L of suspension was transferred to the glassy carbon electrode and dried rapidly under infrared lamp. For continuous coverage, this step was repeated at least five times. Later, the electrode was treated by ozone under ultraviolet radiation lamp (0.9 W) overnight to remove the organic surfactant before running electrochemical measurements. In this study, the author intentionally avoided the use of thermal treatment to remove the surfactant, since high heat is known to cause changes in particle size of nano Au.

Results and Discussions

Morphology

Electron micrographs of Au nanoparticles showed particles with narrow size distribution, as intended from the synthesis approach. Figure 18 (a) is the TEM image of the gold particles on top of lacey carbon. The average size is 3.5 nm, with a

majority of particles ranging from 2.2 nm to 3.8 nm. EDAX shows no presence of either N or Br, indicating the effective washing of the surfactant. The large Cu peak is attributed to the TEM grid, as no Cu was used in the synthesis of the catalyst. For brevity, the following discussions will be limited to Au particles of 3.5 nm.

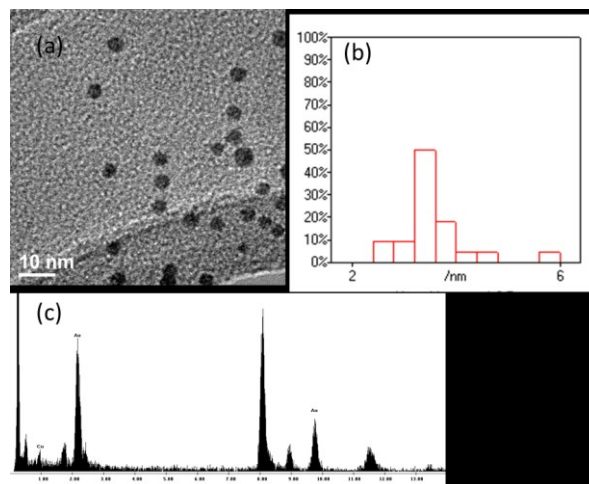


Figure 18 (a) TEM image of free Au particles without carbon support; (b) histogram of Au particles; and (c) EDAX of the particles.

Cyclic Voltammetry

The cyclic voltammograms of Au/C with different scanning potential ranges are summarized in Figure 19. The featureless region is apparent in the voltammogram at potentials of 0.0 to 0.9 V, since Au has no response to hydrogen adsorption or desorption under these conditions. From 0.9 to 1.2 V is the oxide reduction region, and above 1.2 V is the oxide formation region. The degree of Au oxide formation is known to be very sensitive to the sweeping potential [60, 61], and has been shown to correlate to the size of the reduction peak, which is distinctly different when using different sweeping potentials. In addition, the evaluation of active surface area of Au is quite

different from Pt [62]. While some researchers have used a Cu monolayer deposition method [54] to do the evaluation, most studies rely on the reduction peak alone. Assuming the Au surface forms a monolayer of AuO at the potential for oxygen evolution, the empirical charge density of Au is 390 uC/cm^2 [48]. Using this, the surface area can now be determined.

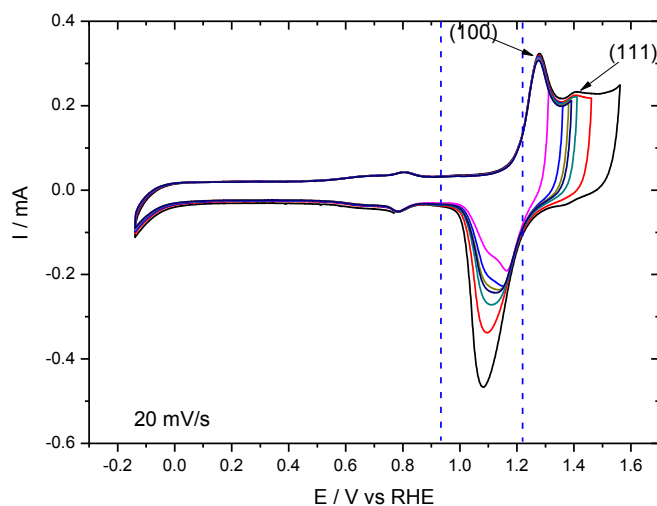


Figure 19 CV of Au/C in 0.1 M KOH with different upper potential, the reduction peak size is proportional to the potential upper limit.

ORR Activity and Durability

To study the kinetics of ORR on Au/C surface, polarization curves at different rotating speeds were taken. These curves are shown in Figure 20 (a) with the background subtracted. The onset potential for the reduction of oxygen is about 0.95 V. The reduction reaches a plateau at 0.75 V before shifting slightly, due to the peroxide production. The inset (b) in Figure 20 presents a plot of i^{-1} vs $\omega^{-0.5}$ for various potentials. The slope equals $6.73 \text{ cm}^2 \cdot \text{rpm}^{0.5} / \text{mA}$, which is in good agreement with the accepted literature value of $7.0 \text{ cm}^2 \cdot \text{rpm}^{0.5} / \text{mA}$ for a four electron ($n=4$) process based

on O₂ solubility [63]. This suggests improved efficiency of nano-Au compared to the traditional bulk-sized Au material.

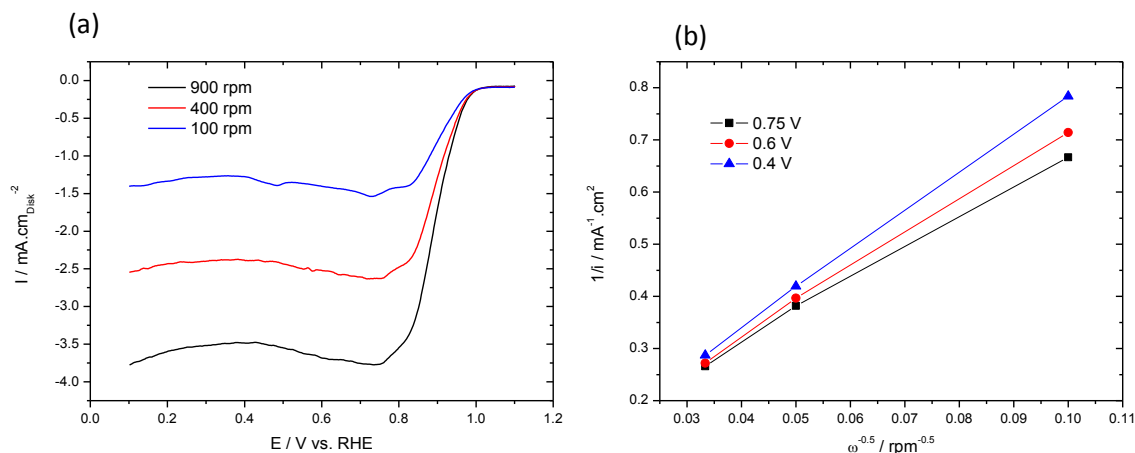


Figure 20 (a) ORR polarization curves at different rotation speed with sweeping rate 50 mV/s; (b) Levich-Koutecky Plots for the ORR on Au at various potentials extracted from data in (a); current density normalized to the geometric electrode area.

Commercial catalyst, Pt/C, was tested as a bench mark for comparison. The initial activity of Au/C is $0.17 \text{ mA}/\text{cm}^2$, which approximately 60% of that of Pt/C at $0.29 \text{ mA}/\text{cm}^2$. This difference is much smaller than the several orders of magnitude difference between bulk Au and Pt. Next, the accelerated durability test was carried out by cycling the potential from 0.6 V to 1.1 V at 20 mV/s for 2000 cycles. With the help of the slow potential sweeping rate, it was possible to see dramatic differences between the two catalysts. By the end of the durability test, Pt/C had lost 40 % of its initial surface area; meanwhile, Au/C surface area decreased by only 9 %. The improved stability of Au/C catalyst is a result of the inherently higher dissolution

potential. With slower dissolution and redeposition kinetics, Au/C exhibits a much smaller degradation than Pt/C as shown in Figure 21.

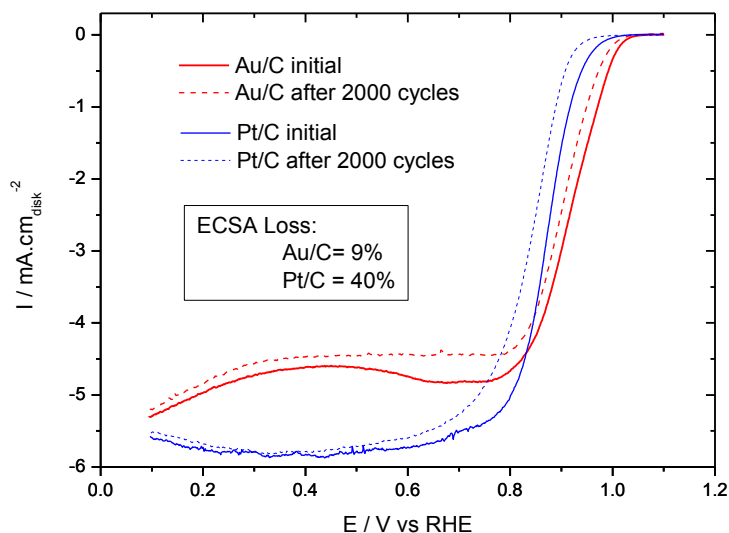


Figure 21 ORR polarization curves of Au/C and Pt/C both at the beginning (solid line) and at the end (dash line) of the durability test with ECSA loss comparison inset.

Summary

Nanoscale Au on C catalyst has been studied in detail. During catalyst synthesis, it was found that solvent washing and ozone treatment is an effective way to remove the surfactant. The only drawbacks of this treatment are the uncertainty in the mass loading of metal on the electrode, and difficulty in applying large amounts of sample. Furthermore, Au/C exhibits activity approaching that of Pt/C, in addition to exceptionally high stability under stressful test conditions. This result is very encouraging for design of catalysts without Pt, as well as development of future Au-based catalyst.

Chapter 5

SUMMARY AND CONCLUSION

In this thesis, the author first discussed and summarized the mechanism and development of the electrochemical reduction of oxygen on Pt and Pt-based catalysts. In the second part, two different types of catalysts were explored for fuel cell application.

The author established a simple wet chemistry method to produce Pt/Sc₂O₃ catalyst via a one-pot synthesis approach. The sheet-like structure of Sc₂O₃ serves as both a support and a protecting structure for Pt nanoparticles, at early stages of durability testing. The tuning effect from the metal-support interaction was demonstrated by XPS analysis. Remarkably, the Pt/Sc₂O₃/C catalyst shows three times higher activity than the commercial Pt/C, under an acidic environment. Furthermore, the ECSA loss of Pt/Sc₂O₃/C after a 30,000-cycles durability test is only one third of Pt/C, demonstrating a much slower degradation rate.

The author also studied the activity of nano Au/C for fuel cell catalysis in alkaline environments. Au/C with narrow size distribution was produced under mild reaction conditions. Performance suggests that the catalyst utilized a 4-electron transfer process during the reduction of oxygen. In addition, Au/C demonstrated comparable activity to that of the commercial Pt/C. With a much higher dissolution potential, the Au/C catalyst proved to be the more stable catalyst. Durability tests showed only 9 % of the initial surface loss in Au/C, compared to that of 40 % in commercial Pt/C.

The improved activity and enhanced stability of the catalysts just discussed provide useful information for further research into fuel cell catalysis. Furthermore, large scale catalyst synthesis should be carried out so that fuel cell MEA testing with PEM or HEM can be performed, providing the stepping stones for commercialization.

REFERENCES

1. Steele, B.C.H. and A. Heinzel, *Materials for fuel-cell technologies*. Nature, 2001. **414**(6861): p. 345-352.
2. Borup, R., et al., *Scientific aspects of polymer electrolyte fuel cell durability and degradation*. Chemical Reviews, 2007. **107**(10): p. 3904-3951.
3. Gasteiger, H.A., et al., *Activity benchmarks and requirements for Pt, Pt-alloy, and non-Pt oxygen reduction catalysts for PEMFCs*. Applied Catalysis B-Environmental, 2005. **56**(1-2): p. 9-35.
4. Gu, S., et al., *An efficient Ag-ionomer interface for hydroxide exchange membrane fuel cells*. Chemical Communications, 2013. **49**(2): p. 131-133.
5. Gu, S., et al., *Quaternary Phosphonium-Based Polymers as Hydroxide Exchange Membranes*. Chemsuschem, 2010. **3**(5): p. 555-558.
6. Gu, S., et al., *A Soluble and Highly Conductive Ionomer for High-Performance Hydroxide Exchange Membrane Fuel Cells*. Angewandte Chemie-International Edition, 2009. **48**(35): p. 6499-6502.
7. Gong, K.P., et al., *Nitrogen-Doped Carbon Nanotube Arrays with High Electrocatalytic Activity for Oxygen Reduction*. Science, 2009. **323**(5915): p. 760-764.
8. Spendelow, J.S. and A. Wieckowski, *Electrocatalysis of oxygen reduction and small alcohol oxidation in alkaline media*. Physical Chemistry Chemical Physics, 2007. **9**(21): p. 2654-2675.
9. Liang, Y.Y., et al., *Co₃O₄ nanocrystals on graphene as a synergistic catalyst for oxygen reduction reaction*. Nature Materials, 2011. **10**(10): p. 780-786.
10. Bligaard, T., et al., *The Bronsted-Evans-Polanyi relation and the volcano curve in heterogeneous catalysis*. Journal of Catalysis, 2004. **224**(1): p. 206-217.
11. Hammer, B. and J.K. Norskov, *Theoretical surface science and catalysis - Calculations and concepts*. Advances in Catalysis, Vol 45, 2000. **45**: p. 71-129.
12. Greeley, J., et al., *Alloys of platinum and early transition metals as oxygen reduction electrocatalysts*. Nature Chemistry, 2009. **1**(7): p. 552-556.
13. Norskov, J.K., et al., *Origin of the overpotential for oxygen reduction at a fuel-cell cathode*. Journal of Physical Chemistry B, 2004. **108**(46): p. 17886-17892.
14. Greeley, J. and J.K. Norskov, *Combinatorial Density Functional Theory-Based Screening of Surface Alloys for the Oxygen Reduction Reaction*. Journal of Physical Chemistry C, 2009. **113**(12): p. 4932-4939.

15. Greeley, J.P., J. Rossmeisl, and J.K. Norskov, *Structure sensitivity and stability of oxygen reduction reaction catalysts from first principles*. Abstracts of Papers of the American Chemical Society, 2007. **233**.
16. Ferreira, P.J., et al., *Instability of Pt/C electrocatalysts in proton exchange membrane fuel cells - A mechanistic investigation*. Journal of The Electrochemical Society, 2005. **152**(11): p. A2256-A2271.
17. Shao-Horn, Y., et al., *Instability of Supported Platinum Nanoparticles in Low-Temperature Fuel Cells*. Topics in Catalysis, 2007. **46**(3-4): p. 285-305.
18. Zhongwei Chen, et al., *Supportless Pt and PtPd Nanotubes as Electrocatalysts for Oxygen-Reduction Reactions*. Angew Chem Int Ed Engl, 2007. **46**(22): p. 4060-4063.
19. Liu, Z., et al., *Atomic-Scale Compositional Mapping and 3-Dimensional Electron Microscopy of Dealloyed PtCo₃ Catalyst Nanoparticles with Spongy Multi-Core/Shell Structures*. Journal of The Electrochemical Society, 2012. **159**(9): p. F554-F559.
20. Mundy, J.A., et al., *Atomic-resolution chemical imaging of oxygen local bonding environments by electron energy loss spectroscopy*. Applied Physics Letters, 2012. **101**(4): p. 042907.
21. Yu, Y., et al., *Three-dimensional tracking and visualization of hundreds of Pt-Co fuel cell nanocatalysts during electrochemical aging*. Nano Lett, 2012. **12**(9): p. 4417-23.
22. Xin, H.L., et al., *Atomic-resolution spectroscopic imaging of ensembles of nanocatalyst particles across the life of a fuel cell*. Nano Lett, 2012. **12**(1): p. 490-7.
23. Toda, T., et al., *Enhancement of the electroreduction of oxygen on Pt alloys with Fe, Ni, and Co*. Journal of The Electrochemical Society, 1999. **146**(10): p. 3750-3756.
24. Paulus, U.A., et al., *Oxygen reduction on carbon-supported Pt-Ni and Pt-Co alloy catalysts*. Journal of Physical Chemistry B, 2002. **106**(16): p. 4181-4191.
25. Stamenkovic, V.R., et al., *Improved oxygen reduction activity on Pt₃Ni(111) via increased surface site availability*. Science, 2007. **315**(5811): p. 493-7.
26. Paffett, M.T., J.G. Beery, and S. Gottesfeld, *Oxygen Reduction at Pt_{0.65}Cr_{0.35}, Pt_{0.2}Cr_{0.8} and Roughened Platinum*. Journal of The Electrochemical Society, 1988. **135**(6): p. 1431-1436.
27. Beard, B.C. and P.N. Ross, *The Structure and Activity of Pt-Co Alloys as Oxygen Reduction Electrocatalysts*. Journal of The Electrochemical Society, 1990. **137**(11): p. 3368-3374.
28. Jalan, V. and E.J. Taylor, *Importance of Interatomic Spacing in Catalytic Reduction of Oxygen in Phosphoric-Acid*. Journal of The Electrochemical Society, 1983. **130**(11): p. 2299-2301.
29. Mukerjee, S., et al., *Role of Structural and Electronic-Properties of Pt and Pt Alloys on Electrocatalysis of Oxygen Reduction - an in-Situ Xanes and Exafs*

- Investigation*. Journal of The Electrochemical Society, 1995. **142**(5): p. 1409-1422.
30. Stamenkovic, V.R., et al., *Trends in electrocatalysis on extended and nanoscale Pt-bimetallic alloy surfaces*. Nature Materials, 2007. **6**(3): p. 241-247.
 31. Greeley, J. and J.K. Nørskov, *Electrochemical dissolution of surface alloys in acids: Thermodynamic trends from first-principles calculations*. Electrochimica Acta, 2007. **52**(19): p. 5829-5836.
 32. Stamenkovic, V., et al., *Surface composition effects in electrocatalysis: Kinetics of oxygen reduction on well-defined Pt₃Ni and Pt₃Co alloy surfaces*. Journal of Physical Chemistry B, 2002. **106**(46): p. 11970-11979.
 33. <effect of surface composition on electronic structure.pdf>.
 34. Greeley, J., *Structural effects on trends in the deposition and dissolution of metal-supported metal adstructures*. Electrochimica Acta, 2010. **55**(20): p. 5545-5550.
 35. Zhang, J.L., et al., *Controlling the catalytic activity of platinum-monolayer electrocatalysts for oxygen reduction with different substrates*. Angewandte Chemie-International Edition, 2005. **44**(14): p. 2132-2135.
 36. Zhang, J.L., et al., *Mixed-metal Pt monolayer electrocatalysts for enhanced oxygen reduction kinetics*. Journal of the American Chemical Society, 2005. **127**(36): p. 12480-12481.
 37. Zhang, J., et al., *Platinum monolayer on nonnoble metal-noble metal core-shell nanoparticle electrocatalysts for O₂ reduction*. Journal of Physical Chemistry B, 2005. **109**(48): p. 22701-22704.
 38. Ruban, A.V., H.L. Skriver, and J.K. Nørskov, *Surface segregation energies in transition-metal alloys*. Physical Review B, 1999. **59**(24): p. 15990-16000.
 39. Huang, S.Y., et al., *Development of a Titanium Dioxide-Supported Platinum Catalyst with Ultrahigh Stability for Polymer Electrolyte Membrane Fuel Cell Applications*. Journal of the American Chemical Society, 2009. **131**(39): p. 13898-+.
 40. Alia, S.M., et al., *Platinum-Coated Palladium Nanotubes as Oxygen Reduction Reaction Electrocatalysts*. Acs Catalysis, 2012. **2**(5): p. 858-863.
 41. di Paola, C. and F. Baletto, *Oxygen adsorption on small PtNi nanoalloys*. Physical Chemistry Chemical Physics, 2011. **13**(17): p. 7701-7707.
 42. Jong Yoo, S., et al., *Enhanced stability and activity of Pt-Y alloy catalysts for electrocatalytic oxygen reduction*. Chem Commun (Camb), 2011. **47**(41): p. 11414-6.
 43. Nesselberger, M., et al., *The particle size effect on the oxygen reduction reaction activity of Pt catalysts: influence of electrolyte and relation to single crystal models*. Journal of the American Chemical Society, 2011. **133**(43): p. 17428-33.

44. Escudero-Escribano, M., et al., *Pt5Gd as a highly active and stable catalyst for oxygen electroreduction*. Journal of the American Chemical Society, 2012. **134**(40): p. 16476-9.
45. Stephens, I.E.L., et al., *Oxygen Electroreduction Activity and X-Ray Photoelectron Spectroscopy of Platinum and Early Transition Metal Alloys*. ChemCatChem, 2012. **4**(3): p. 341-349.
46. Stephens, I.E.L., et al., *Understanding the electrocatalysis of oxygen reduction on platinum and its alloys*. Energy & Environmental Science, 2012. **5**(5): p. 6744.
47. Bezerra, C.W.B., et al., *A review of heat-treatment effects on activity and stability of PEM fuel cell catalysts for oxygen reduction reaction*. Journal of Power Sources, 2007. **173**(2): p. 891-908.
48. Trasatti, S. and O.A. Petrii, *Real Surface-Area Measurements in Electrochemistry*. Pure and Applied Chemistry, 1991. **63**(5): p. 711-734.
49. Wang, C., et al., *Synthesis of Homogeneous Pt-Bimetallic Nanoparticles as Highly Efficient Electrocatalysts*. Acs Catalysis, 2011. **1**(10): p. 1355-1359.
50. Wang, C., et al., *Design and Synthesis of Bimetallic Electrocatalyst with Multilayered Pt-Skin Surfaces*. Journal of the American Chemical Society, 2011. **133**(36): p. 14396-14403.
51. Wang, C., et al., *Monodisperse Pt3Co nanoparticles as electrocatalyst: the effects of particle size and pretreatment on electrocatalytic reduction of oxygen*. Physical Chemistry Chemical Physics, 2010. **12**(26): p. 6933-6939.
52. Alia, S.M., et al., *Porous Platinum Nanotubes for Oxygen Reduction and Methanol Oxidation Reactions*. Advanced Functional Materials, 2010. **20**(21): p. 3742-3746.
53. Haruta, M., *Size- and support-dependency in the catalysis of Gold*. Catalysis Today, 1997.
54. Wei Tang, Galen D. Stucky, and E.W. McFarland, *Size-Dependent Activity of Gold Nanoparticles for Oxygen Electroreduction in Alkaline Electrolyte*. J. Phys. Chem. C, 2008.
55. Hernandez, J., et al., *Electrochemistry of Shape-Controlled Catalysts: Oxygen Reduction Reaction on Cubic Gold Nanoparticles*. J. Phys. Chem. C, 2007.
56. Chen, W. and S. Chen, *Oxygen electroreduction catalyzed by gold nanoclusters: strong core size effects*. Angew Chem Int Ed Engl, 2009. **48**(24): p. 4386-9.
57. El-Deab, M.S., T. Okajima, and T. Ohsaka, *Electrochemical Reduction of Oxygen on Gold Nanoparticle-Electrodeposited Glassy Carbon Electrodes*. Journal of The Electrochemical Society, 2003. **150**(7): p. A851.
58. Yagi, I., T. Ishida, and K. Uosaki, *Electrocatalytic reduction of oxygen to water at Au nanoclusters vacuum-evaporated on boron-doped diamond in acidic solution*. Electrochemistry Communications, 2004. **6**(8): p. 773-779.
59. Peng, S., et al., *A facile synthesis of monodisperse Au nanoparticles and their catalysis of CO oxidation*. Nano Research, 2008. **1**(3): p. 229-234.

60. Hamelin, A., *Cyclic Voltammetry at Gold Single Crystal Surfaces*. Journal of Electroanalytical Chemistry, 1996.
61. Burke, L.D., J.M. Moran, and P.F. Nugent, *Cyclic voltammetry responses of metastable gold electrodes in aqueous media*. Journal of Solid State Electrochemistry, 2003. **7**(9): p. 529-538.
62. Trasatti, S. and O.A. PeterII, *Real Surface Area Measurements in Electrochemistry*. .I. Electroanal. Chem., 1992.
63. Gubbins, K.E. and R.D. Walker, *Solubility and Diffusivity of Oxygen in Electrolytic Solutions*. Journal of The Electrochemical Society, 1965. **112**(5): p. 469-&.